PAPER

Antenna Array Calibration Based on Frequency Selection in OFDMA/TDD Systems

Yoshitaka HARA[†a)], **Yasuhiro YANO**[†], *and* **Hiroshi KUBO**[†], *Members*

SUMMARY This paper proposes a new antenna array calibration technique which uses frequency selection in orthogonal frequency division multiple access (OFDMA)/time division duplexing (TDD) systems. In the proposed method, subbands or frequencies of good channel conditions are initially selected for channel measurements. The relative calibration is performed at the selected subbands, which compensates for mismatch of analogue gains in multiple antennas using the measured uplink and downlink channel parameters. Furthermore, the calibration parameters are interpolated in the frequency domain for the whole bandwidth. The proposed calibration maintains accurate channel reciprocity for the whole bandwidth compared to the conventional calibration which does not use the frequency selection. The proposed calibration technique is effective in exploiting channel reciprocity at both base station and terminals with feasible amount of feedback and low-cost operation.

key words: *wireless communications, OFDMA, TDD, calibration, antenna arrays, MIMO, channel reciprocity*

1. Introduction

Wireless transmission schemes using multiple antennas have been widely investigated to meet the growing demands for high data rate communications. In specific, transmit beamforming technique is important for a base station (BS) to transmit signals to different terminals simultaneously based on space division multiplexing (SDM) [1]. Transmit beamforming is also essential for terminals to reduce transmit power on uplink.

For efficient transmit beamforming, time division duplexing (TDD) system has an advantage in exploiting channel reciprocity between uplink and downlink. In TDD systems with ideal channel reciprocity, a transceiver can obtain downlink (uplink) channel knowledge from uplink (downlink) channel measurements. Therefore, an appropriate transmit beam can be formed based on the channel measurement results without any feedback information. However, in actual environments, the measured uplink and downlink channel parameters are not identical due to different gains of analogue devices in transmit and receive circuits. Thus, an antenna array calibration technique, which compensates for mismatch of analogue gains in multiple antennas, is necessary to exploit channel reciprocity.

While most existing calibrations [2]–[5] are costly due to extra analogue processing, a low-cost calibration technique applicable to a terminal with multiple antennas is desirable for future wireless systems. The papers [6]–[8] have so far presented a low-cost relative calibration, which compensates for mismatch of analogue gains in multiple antennas based on uplink and downlink channel measurements. More precisely, the calibration parameter in the relative calibration is given by the radio of measured uplink and downlink channel parameters. Although this technique can be achieved inexpensively by digital signal processing only, its calibration accuracy has not been precisely examined yet. Furthermore, the previous papers have dealt with calibration in a single frequency. A wideband calibration technique for orthogonal frequency division multiple access (OFDMA)/TDD systems in selective fading environments has not been studied yet.

In this paper, we propose an efficient antenna array calibration technique for OFDMA/TDD systems, which improves the performance of the conventional relative calibration. In the proposed method, subbands or frequencies of good channel conditions are selected for channel measurements and the relative calibration is applied at the selected subbands. The obtained calibration parameters are interpolated in the frequency domain for the whole bandwidth. We demonstrate that the proposed method improves the performance of the conventional relative calibration for the whole bandwidth while using low-cost digital processing with feasible amount of feedback information. It should be noted that the previous investigations have not dealt with frequency selection for channel measurements.

There are two main approaches in antenna array calibrations. The first approach is the relative calibration technique [6]–[8] mentioned above which transmits (receives) calibration signals to (from) another wireless node. This approach is robust to power-dependent analogue characteristics, because the calibration signal is transmitted with the same power as data signal. However, its calibration accuracy degrades considerably when channel measurements are not accurate. The second approach is self-calibration technique [2]–[5], [9] in which calibration signals are exchanged among antennas of a wireless node. Contrary to the relative calibration, self-calibration does not need feedback from other wireless nodes. In addition, the self-calibration technique exhibits excellent calibration accuracy assuming that analogue characteristics of the node do not depend on transmit power level. However, performance of the self-calibration technique deteriorates when multiple antennas have different power-dependent analog characteristics. Although the aforementioned performance deterioration can

Manuscript received December 5, 2008.
Manuscript revised May 11, 2009.

[†]The authors are with Mitsubishi Electric Corporation, Kamakura-shi, 247-8501 Japan.
a) E-mail: Hara.Yoshitaka@cs.MitsubishiElectric.co.jp

DOI: 10.1587/transcom.E92.B.3195

be reduced by using predetermined table of analogue nonlinearity, further performance degradation is possible due to changes in analogue characteristics of a terminal over many years. In our view, these two approaches have their own properties and need further investigations towards future wireless systems. The rest of this paper focuses on relative calibration since further comparison of the two approaches is beyond the scope of this paper.

This paper is organized as follows. In Sect. 2, system model is described. In Sect. 3, the relative calibration and its natural extension are discussed. In Sect. 4, we propose a new antenna array calibration technique for OFDMA/TDD systems. In Sect. 5, performance of the proposed method is evaluated and Sect. 6 gives the conclusion.

2. System Model

2.1 Signal Model

Figure 1 shows the signal transmission model in TDD systems. In wireless communication systems, channel parameters are usually measured in digital fields through pilot signal transmission. Assume that the BS's n-th antenna has the analogue complex gain $T_{BS,n}$ at the transmit circuit and the analogue complex gain $R_{BS,n}$ at the receive circuit. Likewise, the terminal's m-th antenna has the transmit analogue gain $T_{MT,m}$ and the receive analogue gain $R_{MT,m}$.

In TDD systems, a terminal transmits an uplink signal using carrier frequency which is acquired through downlink signal. Then, the terminal's carrier frequency f_{MT} is so close to the BS's carrier frequency f_{BS} that analogue gains and channel parameters are almost constant between f_{MT} and f_{BS}. Then, the measured uplink channel parameter $h_{m,n}^{(UL)}$ and downlink channel parameter $h_{m,n}^{(DL)}$ between the terminal's m-th antenna and the BS's n-th antenna are expressed as [6]–[10]

$$h_{m,n}^{(UL)} = T_{MT,m} \cdot g_{m,n}^{(UL)} \cdot R_{BS,n} \cdot \exp\{j2\pi(f_{MT} - f_{BS}^{'})t + \phi_{UL}\} \quad (1)$$

$$h_{m,n}^{(DL)} = T_{BS,n} \cdot g_{m,n}^{(DL)} \cdot R_{MT,m} \cdot \exp\{j2\pi(f_{BS} - f_{MT})t + \phi_{DL}\} \quad (2)$$

where $g_{m,n}^{(UL)}$ and $g_{m,n}^{(DL)}$ are the real channel parameters on uplink and downlink, respectively, $f_{BS}^{'}$ is the BS's carrier frequency for signal reception, ϕ_{UL} is the initial phase on uplink, and ϕ_{DL} is the initial phase on downlink. The carrier frequency here is defined as total converted frequency in analogue and digital fields. The BS's carrier frequency $f_{BS}^{'}$ for signal reception is not necessarily identical to f_{BS} for signal transmission due to different frequency control in digital fields.

According to electromagnetic theory, real channel parameters in static channels are reciprocal [8], [11], i.e., $g_{m,n}^{(DL)} = g_{m,n}^{(UL)}$, even in the presence of reflections and coupling between antennas. Meanwhile, the measured channel parameters are not reciprocal, i.e. $h_{m,n}^{(DL)} \neq h_{m,n}^{(UL)}$, due to independent analogue complex gains $T_{BS,n}$, $T_{MT,m}$, $R_{BS,n}$, and $R_{MT,m}$. Hence, an antenna array calibration technique, which compensates for mismatch of the independent analogue gains, is needed to exploit channel reciprocity in TDD systems.

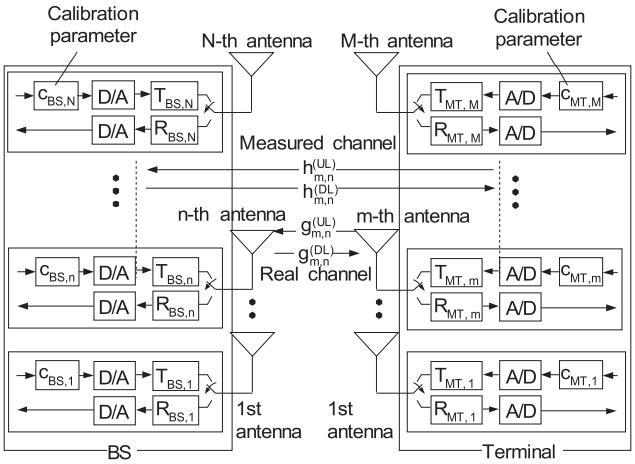

Fig. 1 Signal transmission model in a TDD system.

2.2 Basic Characteristics of Analogue Equipments

We describe basic characteristics of analogue equipments at a wireless transceiver. The analogue complex gains $T_{MT,m}$, $R_{MT,m}$, $T_{BS,n}$, $R_{BS,n}$ are dependent on various factors, such as delay in radio frequency (RF) path, phase rotation in amplifier, and other characteristics of analogue devices. In general, $T_{MT,m}$, $R_{MT,m}$, $T_{BS,n}$, and $R_{BS,n}$ are very slowly time-varying depending on temperature [12]. Therefore, it is reasonable to assume constant analogue gains during a calibration or data packet transmission (< 100 ms).

The amplitude of each analogue device's complex gain is almost constant within a bandwidth which is sufficiently smaller than the carrier frequency. For instance, analogue complex gain has almost constant amplitude within bandwidth 10 MHz at carrier frequency 4 GHz. In the meantime, phase rotation of analogue complex gain occurs in frequency domain due to group delay caused by RF path and analogue devices. In a typical example, 1 m RF path or 3.3 ns group delay causes 1.2° phase rotation per MHz. Thus, the total analogue gains $T_{MT,m}$, $R_{MT,m}$, $T_{BS,n}$, and $R_{BS,n}$ have linear phase rotation in proportion to the operating frequency whilst keeping constant envelopes. The analogue gains $T_{MT,m}$, $R_{MT,m}$, $T_{BS,n}$, $R_{BS,n}$ are also dependent on transmit power level. In general, power dependence becomes remarkable as transmit power level increases. In this paper, we discuss calibration performance based on the above analogue characteristics.

3. Relative Calibration

In this section, we discuss the relative calibration [6]–[8] and its natural extension at a specific frequency.

3.1 Calibration Condition in a MIMO Channel

Let us consider the BS with N antennas and the terminal with M antennas. In the relative calibration, mismatch of analogue complex gains is compensated by multiplying complex calibration parameter $c_{BS,n}$ or $c_{MT,m}$ to transmit signal at the BS's n-th antenna ($n = 1, \ldots, N$) or at the terminal's m-th antenna ($m = 1, \ldots, M$), respectively, as shown in Fig. 1. Then, the measured uplink and downlink channel parameters after calibration are given by

$$a_{m,n}^{(UL)} = c_{MT,m} \cdot h_{m,n}^{(UL)} \tag{3}$$

$$a_{m,n}^{(DL)} = c_{BS,n} \cdot h_{m,n}^{(DL)} \tag{4}$$

respectively. In order to exploit channel reciprocity in a $N \times M$ multiple-input multiple-output (MIMO) channel, it is required to satisfy

$$\eta \equiv \frac{a_{1,1}^{(UL)}}{a_{1,1}^{(DL)}} = \frac{a_{m,n}^{(UL)}}{a_{m,n}^{(DL)}} \tag{5}$$

for all combinations of $m = 1, \ldots, M$ and $n = 1, \ldots, N$. In (5), $a_{m,n}^{(UL)}/a_{m,n}^{(DL)}$ for any (m, n) needs to have the same phase, but the same phase in $a_{m,n}^{(UL)}$ and $a_{m,n}^{(DL)}$ is not required. Even though η has time-variant phase rotation due to carrier frequency offset between the BS and the terminal, the terminal can perform appropriate transmit beamforming if (5) holds. We refer to the condition of (5) as "wide-sense channel reciprocity" and the condition of $a_{m,n}^{(UL)} = a_{m,n}^{(DL)}$ as "strict-sense channel reciprocity." This paper discusses calibration technique which maintains the wide-sense channel reciprocity for transmit beamforming.

Using (1) and (2), (5) is equivalent to the following two equations :

$$\frac{c_{MT,1}T_{MT,1}}{R_{MT,1}} = \frac{c_{MT,2}T_{MT,2}}{R_{MT,2}} = \ldots = \frac{c_{MT,M}T_{MT,M}}{R_{MT,M}} \tag{6}$$

$$\frac{c_{BS,1}T_{BS,1}}{R_{BS,1}} = \frac{c_{BS,2}T_{BS,2}}{R_{BS,2}} = \ldots = \frac{c_{BS,N}T_{BS,N}}{R_{BS,N}}. \tag{7}$$

Furthermore, (6) and (7) are equivalent to the following equations (8) and (9), respectively.

$$\frac{a_{1,1}^{(UL)}}{a_{1,1}^{(DL)}} = \frac{a_{2,1}^{(UL)}}{a_{2,1}^{(DL)}} = \cdots = \frac{a_{M,1}^{(UL)}}{a_{M,1}^{(DL)}} \tag{8}$$

$$\frac{a_{1,1}^{(UL)}}{a_{1,1}^{(DL)}} = \frac{a_{1,2}^{(UL)}}{a_{1,2}^{(DL)}} = \cdots = \frac{a_{1,N}^{(UL)}}{a_{1,N}^{(DL)}} \tag{9}$$

If the BS and the terminal individually meet (8) and (9) in a multiple-input single-output (MISO) channel, the condition of wide-sense channel reciprocity (5) naturally holds. From (8) and (9), it is sufficient to update the complex calibration parameters $c_{MT,m}$ slowly according to variation of analogue gains, e.g. every 5 minutes.

The condition in (5) is different from calibration technique for direction of arrival (DOA) estimation, e.g. [13], which requires $R_{MT,1} = \cdots = R_{MT,M}$. Since it is not necessary to identify DOA in wireless communications, the antenna array calibration technique can be simplified.

3.2 Relative Calibration in a MISO Channel

According to the above discussions, wide-sense channel reciprocity holds in a MIMO channel if the BS and the terminal keep (8) and (9) individually in a MISO channel. Since calibration procedure is the same for the BS and the terminal, we hereafter focus on calibration of the terminal's M antennas in a MISO channel with $N = 1$. In the relative calibration [6], [8], the complex calibration parameter $c_{MT,m}$ is determined as follows :

[Relative calibration for the m-th antenna]

1. Initialize $c_{BS,1} = c_{MT,m} = 1$
2. The terminal transmits a calibration pilot signal from the m-th antenna. The BS measures uplink channel parameter $\hat{a}_{m,1}^{(UL)}$ of
   $$\hat{a}_{m,1}^{(UL)} = h_{m,1}^{(UL)} + \hat{z}_{BS}$$
   where $\hat{z}_{BS}$ denotes the remaining noise in the measured uplink channel parameter.
3. The BS transmits a calibration pilot signal. The terminal measures the channel parameter $\hat{a}_{m,1}^{(DL)}$ at the m-th antenna as
   $$\hat{a}_{m,1}^{(DL)} = h_{m,1}^{(DL)} + \hat{z}_{MT,m}$$
   where $\hat{z}_{MT,m}$ denotes the remaining noise in the measured downlink channel parameter at the terminal's m-th antenna.
4. The BS reports $\hat{a}_{m,1}^{(UL)}$ to the terminal.
5. The terminal determines the calibration parameter as $\hat{c}_{MT,m} = \hat{a}_{m,1}^{(DL)}/\hat{a}_{m,1}^{(UL)}$.

This calibration is applied to a low-mobility terminal. The steps 2. and 3. are performed in a short duration in which channel variation is negligible. The same calibration is performed simultaneously for all antennas ($m = 1, \ldots, M$), using orthogonal pilot sequences or other subcarriers.

The relative calibration has advantages in low-cost digital operation and negligible influence of power-dependent amplifiers. In practice, it is essential to keep accurate channel measurements in fading environments, although the previous papers have not dealt with the relative calibration in fading environments.

4. Calibration for OFDMA/TDD Systems

We propose a new antenna array calibration technique for OFDMA/TDD systems, which maintains wide-sense channel reciprocity with good accuracy in selective fading environments.

4.1 Calibration for OFDMA/TDD Systems

In OFDMA/TDD systems, the analogue complex gains

$T_{MT,m}$, $R_{MT,m}$, $T_{BS,n}$, and $R_{BS,n}$ are dependent on frequency. The ideal calibration parameter $c_{MT,m}(f)$ $(m = 1, \ldots, M)$ in frequency f is expressed as

$$c_{MT,m}(f) = \frac{a^{(DL)}_{m,1}(f)}{a^{(UL)}_{m,1}(f)} = \left| \frac{T_{BS,n}(f)/R_{BS,n}(f)}{T_{MT,m}(f)/R_{MT,m}(f)} \right| \cdot \xi(t) \cdot e^{j\theta(f)} \quad (10)$$

with

$$\theta(f) = \angle T_{BS,n}(f) - \angle R_{BS,n}(f) - \angle T_{MT,m}(f) + \angle R_{MT,m}(f)$$

$$\xi(t) = \frac{e^{j2\pi(f_{BS}-f_{MT})t+\phi_{DL}}}{e^{j2\pi(f_{MT}-f'_{BS})t+\phi_{UL}}}$$

where $\angle x$ denotes the angle of complex value x in $[-\pi, \pi)$, $a^{(DL)}_{m,1}(f)$, $a^{(UL)}_{m,1}(f)$, $T_{MT,m}(f)$, $R_{MT,m}(f)$, $T_{BS,n}(f)$, $R_{BS,n}(f)$ represent $a^{(DL)}_{m,1}$, $a^{(UL)}_{m,1}$, $T_{MT,m}$, $R_{MT,m}$, $T_{BS,n}$, $R_{BS,n}$ in frequency f, respectively. Note that $\xi(t)$ is independent of frequency f.

As presented in **2.2**, the phase $\theta(f)$ is a linear function of frequency f due to group delay in RF cable and analogue circuits, while the envelope $|(T_{BS,n}(f)/R_{BS,n}(f))/(T_{MT,m}(f)/R_{MT,m}(f))|$ is constant. If the BS and the terminal have similar delay in transmit and receive RF paths, the phase rotation is slow in the frequency domain[†]. In this case, calibration parameter is effectively interpolated in the frequency domain. Accordingly, we propose a new calibration technique which uses frequency selection for OFDMA/TDD systems as follows:

[Calibration for OFDMA/TDD Systems]

1. At time instant t, select L frequencies $f^{(1)}_m$, $f^{(2)}_m$, …, $f^{(L)}_m$ $(f^{(l)}_m < f^{(l+1)}_m)$ for the m-th antenna $(m = 1, \ldots, M)$ among
$$f = F_0, F_0 + B, F_0 + 2B, \ldots, F_0 + (LM - 1)B \quad (11)$$
where F_0 is the initial frequency and B is the minimum frequency interval.
2. Compute the calibration parameters $\hat{c}_{MT,m}(f^{(1)}_m, t)$, $\hat{c}_{MT,m}(f^{(2)}_m, t)$, …, $\hat{c}_{MT,m}(f^{(L)}_m, t)$ at the selected L frequencies for the m-th antenna $(m = 1, \ldots, M)$ using the relative calibration.
3. Determine the calibration parameter $c_{MT,m}(f, t)$ for the whole bandwidth based on frequency-domain interpolation.
4. Repeat the steps 1. to 3. at $t = 1, \ldots, T$. Compute the refined calibration parameter $c_{MT,m}(f)$ from $c_{MT,m}(f, 1), \ldots, c_{MT,m}(f, T)$.

In step 4., T time instants $t = 1, \ldots, T$ are chosen in a duration of constant analogue gains. The proposed method is expected to keep good calibration accuracy, selecting appropriate frequencies for channel measurements. The details of steps 1., 3., and 4. are explained in **4.2**, **4.3**, and **4.4**, respectively.

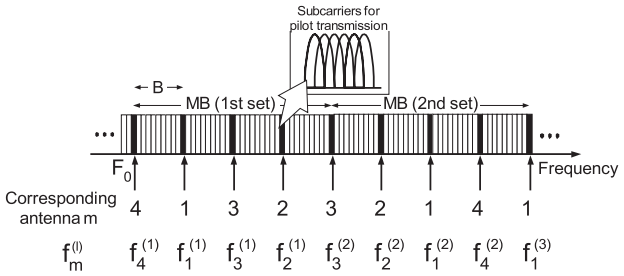

Fig. 2 An example of mapping frequencies into antennas for the proposed calibration in OFDMA ($M = L = 4$).

4.2 Frequency Selection in Step 1

In step 1, $f^{(l)}_1, f^{(l)}_2, \ldots, f^{(l)}_M$ are selected without overlapping from a set of M frequencies

$$\boldsymbol{F}^{(l)} = \{F_0 + (l-1)MB + (m-1)B | m = 1, \ldots, M\}$$

such that each antenna has good channel condition. This frequency selection is performed independently for different l. Figure 2 shows the example of mapping frequencies into antennas in the proposed calibration.

In this allocation, the terminal initially measures the channel parameters $\hat{a}^{(DL)}_{m,1}(f)$ $(f \in \boldsymbol{F}^{(l)})$ at all antennas $m = 1, \ldots, M$ using downlink common pilot signal. Next, among $M!$ possibilities of mapping $\boldsymbol{F}^{(l)}$ into $f^{(l)}_1, f^{(l)}_2, \ldots, f^{(l)}_M$, the terminal selects $f^{(l)}_1, f^{(l)}_2, \ldots, f^{(l)}_M$ which maximizes J of

$$J = \begin{cases} \sum_{m=1}^{M} \log_{10} |\hat{a}^{(DL)}_{m,1}(f^{(l)}_m)| & \text{in allocation 1} \\ \sum_{m=1}^{M} |\hat{a}^{(DL)}_{m,1}(f^{(l)}_m)| & \text{in allocation 2} \\ \sum_{m=1}^{M} |\hat{a}^{(DL)}_{m,1}(f^{(l)}_m)|^2 & \text{in allocation 3.} \end{cases} \quad (12)$$

In (12), functions J are chosen to examine three types of allocation strategies. The function J in allocation 1 gives a great negative value to small $\hat{a}^{(DL)}_{m,1}(f^{(l)}_m)$, which prevents the terminal from selecting poor channels with high priority. Meanwhile, J in allocation 3 gives a great positive value to large $\hat{a}^{(DL)}_{m,1}(f^{(l)}_m)$ which prioritizes use of good channels. Appendix A reveals that allocation 1 selects a set of less variant channels than allocations 2 and 3. Maximization of J is performed independently for different l.

The BS can report the measured uplink channel parameter in response to an uplink calibration pilot signal without knowing the frequency allocation. Therefore, CAL2 does

[†]In case of (BS's Tx RF path+terminal's Rx RF path)−(terminal's Tx RF path+BS's Rx RF path) = dm, phase rotation of $\theta(f)$ is $1.2d°$/MHz.

not require any additional control signalling between the BS and the terminal. CAL1 and CAL2 have the same amount of control signalling.

4.3 Interpolation of Calibration Parameters in Step 3

In step 3., the terminal computes the complex calibration parameter $c_{MT,m}(f,t)$ for the whole bandwidth based on linear phase interpolation of $\hat{c}_{MT,m}(f_m^{(l)},t)$. The parameter $c_{MT,m}(f,t)$ ($f_m^{(l)} \le f < f_m^{(l+1)}$, $l = 1,\ldots,L-1$) is determined by

$$|c_{MT,m}(f,t)| = |\hat{c}_{MT,m}(f_m^{(l)},t)| + \frac{f-f_m^{(l)}}{f_m^{(l+1)}-f_m^{(l)}}\left|\frac{\hat{c}_{MT,m}(f_m^{(l+1)},t)}{\hat{c}_{MT,m}(f_m^{(l)},t)}\right| \quad (13)$$

$$\angle c_{MT,m}(f,t) = \angle\hat{c}_{MT,m}(f_m^{(l)},t) + \frac{f-f_m^{(l)}}{f_m^{(l+1)}-f_m^{(l)}}\angle\left(\frac{\hat{c}_{MT,m}(f_m^{(l+1)},t)}{\hat{c}_{MT,m}(f_m^{(l)},t)}\right). \quad (14)$$

The parameter $c_{MT,m}(f,t)$ for $f < f_m^{(1)}$ or $f \ge f_m^{(L)}$ is given by setting $l = 1$ or $l = L-1$ in (13) and (14), respectively. The phase interpolation in (14) matches with linear phase rotation in analogue fields.

4.4 Refinement of Calibration Parameters in Step 4

In step 4., the terminal computes the refined calibration parameter $c_{MT,m}(f)$ using $c_{MT,m}(f,t)$ ($t = 1,\ldots,T$) as

$$\frac{1}{T}\sum_{t=1}^{T}\left\{\frac{\boldsymbol{c}_{MT}^{\dagger}(f,t)}{\|\boldsymbol{c}_{MT}^{\dagger}(f,t)\|}\frac{\boldsymbol{c}_{MT}(f,T)}{\|\boldsymbol{c}_{MT}(f,T)\|}\cdot\boldsymbol{c}_{MT}(f,t)\right\} \to \boldsymbol{c}_{MT}(f) \quad (15)$$

with

$$\boldsymbol{c}_{MT}(f,t) = [c_{MT,1}(f,t),\ldots,c_{MT,M}(f,t)]^T$$
$$\boldsymbol{c}_{MT}(f) = [c_{MT,1}(f),\ldots,c_{MT,M}(f)]^T$$

where † denotes the complex conjugate transpose and ^{T} denotes the transpose. Since all elements in $\boldsymbol{c}_{MT}(f,t)$ have the same time-variant phase rotation $\xi(t)$ due to carrier frequency offset, the phase difference between two time instants t and T is estimated by $(\boldsymbol{c}_{MT}^{\dagger}(f,t)/\|\boldsymbol{c}_{MT}(f,T)\|)(\boldsymbol{c}_{MT}(f,T)/\|\boldsymbol{c}_{MT}(f,T)\|)$. In (15), the estimated phase difference is used to compensate for the phase rotation in $\boldsymbol{c}_{MT}(f,t)$. Thus, the calibration parameters at different time instants can be phase-aligned. This refinement process is expected to improve calibration accuracy even in the presence of frequency offset.

5. Performance Evaluation

The proposed calibration is evaluated by simulations.

Table 1 Simulation parameters.

System	OFDMA/TDD system
System bandwidth	88 MHz
FFT size	8192
Number of used subcarriers	6600
Frequency spacing of subcarrier	13.333 kHz
Frequency interval for calibration pilot signals	B = 1 MHz 75 subcarriers
Number of allocated subbands for one antenna's calibration	L = 22
Channel	Rayleigh channel (Delay spread τ = 0.1, 0.5, 1.0 μs)
Number of antennas at terminal	M = 4
Frequency offsets	$\lvert f_{MT} - f_{BS}^{'}\rvert \le 20$ Hz $\lvert f_{BS} - f_{MT}\rvert \le 20$ Hz

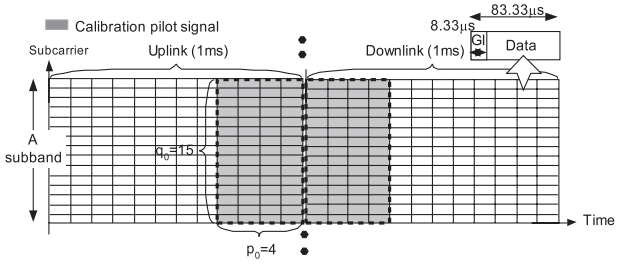

Fig. 3 Calibration pilot symbols in an OFDMA/TDD system.

5.1 Simulation Parameters

Table 1 lists simulation parameters. Figure 3 shows the arrangement of calibration pilot signals in our testbed frame format for OFDMA/TDD system [1]. The frame format contains 6600 subcarriers with subcarrier spacing 13.33 kHz in system bandwidth 88 MHz. Each uplink and downlink frame contains 12 time symbols in 1ms. This symbol format is close to that in Third Generation Partnership Project (3GPP) — Long Term Evolution (LTE) specification [14] where 14 time symbols are arranged with subcarrier spacing 15 kHz in 1ms duration. We consider wider system bandwidth than LTE system to study advanced wireless system towards International Mobile Telecommunication (IMT)-advanced. When uplink is switched to downlink, guard period is not needed because the BS's switching time from reception to transmission is usually much smaller than cyclic prefix [14], [15]†.

The calibration pilot signals are arranged every B = 1 MHz in a rectangular area of $p_0 = 4$ symbols in the time domain and $q_0 = 15$ subcarriers in the frequency domain, i.e. total $p_0 q_0 = 60$ symbols. The bandwidth of $q_0 = 15$ subcarriers is referred to as a subband. The uplink and downlink channels are measured by correlating the received signal and the calibration pilot signal in time and frequency domain. In exact sense, frequency $f_m^{(l)}$ represents the center frequency of the subband for the calibration pilot signal.

†When downlink is switched to uplink, guard period is needed to cope with round trip propagation delay.

In computer simulations, calibration is performed in MISO channel between the terminal's $M = 4$ antennas and the BS's reference antenna ($n = 1$). Quasi-static Rayleigh faded multipath channel is assumed, where uplink and the following downlink have a static fading channel with exponentially decay power profile of delay spread $\tau = 0.1, 0.5, 1.0\,\mu s$. The fading channel is independent between the terminal's antennas. We assume $P_{BS,s}/P_{MT,z} = P_{MT,s}/P_{BS,z} = \text{SNR}$ in simulations, where $P_{BS,s}$ denotes the BS's transmit power for a calibration pilot symbol, $P_{BS,z}$ is the BS's noise power, $P_{MT,s}$ is the terminal's transmit power for a calibration pilot symbol in each antenna, and $P_{MT,z}$ is the terminal's noise power. Exact signal transmission model is expressed in (A· 2) of Appendix B.

In the proposed method, the BS measures the uplink channel parameter $\hat{a}^{(UL)}_{m,1}(f^{(l)}_m)$ ($l = 1, \ldots, L$, $m = 1, \ldots, M$) at the BS's reference antenna ($n = 1$). The BS reports $\hat{a}^{(UL)}_{m,1}(f^{(l)}_m)$ to the terminal after quantizing the common parameter $A = (1/ML)\sum_{m=1}^{M}\sum_{l=1}^{L}|\hat{a}^{(UL)}_{m,1}(f^{(l)}_m)|^2$ of -171 dBm to 20 dBm into 6 bits (3 dB/bit), each instantaneous parameter $|\hat{a}^{(UL)}_{m,1}(f^{(l)}_m)|^2 - A$ of -20 dB to 10 dB into 8 bits (0.117 dB/bit), and $\angle\hat{a}^{(UL)}_{m,1}(f^{(l)}_m)$ into 10 bits (0.35°/bit) for each $l = 1, \ldots, L$ and $m = 1, \ldots, M$. Using this quantization model, we can study feasibility of the proposed calibration in terms of amount of signalling.

The analogue complex gains $T_{MT,m}(f)$, $R_{MT,m}(f)$, $T_{BS,n}(f)$, $R_{BS,n}(f)$ are assumed to have constant envelope and linear phase rotations of 3°, 5.25°, 6°, 3° per 1 MHz in the frequency domain, respectively[†]. Considering that $\theta(f)$ in (10) has phase rotation 2.25°/MHz with this assumption, it is reasonable to interpolate calibration parameters using average frequency interval 4 MHz, i.e., interpolation for average phase rotation 10°. Accordingly, calibration pilot signals are arranged at $L = 22$ subbands for one antenna in 88 MHz.

In performance evaluation, the average phase error after calibration is defined as

$$\Delta\phi = \left\langle \epsilon^2 \right\rangle^{0.5}$$

with the instantaneous phase error ϵ given by

$$\begin{aligned}\epsilon &= \left| \angle\left(\frac{a^{(UL)}_{m_1,1}}{a^{(DL)}_{m_1,1}}\right) - \angle\left(\frac{a^{(UL)}_{m_2,1}}{a^{(DL)}_{m_2,1}}\right)\right| \quad m_1 \neq m_2 \\ &= \left| \angle\left(\frac{c_{MT,m_1}(f)T_{MT,m_1}(f)/R_{MT,m_1}(f)}{c_{MT,m_2}(f)T_{MT,m_2}(f)/R_{MT,m_2}(f)}\right)\right|\end{aligned}$$

where $\langle\cdot\rangle$ denotes the average over all combinations of m_1, m_2 and frequency f in the whole bandwidth. In addition, 99 percentile phase error is defined as ϵ_{th} which satisfies

$$\Pr[\epsilon < \epsilon_{th}] = 0.99 \tag{16}$$

where $\Pr[\epsilon < \epsilon_{th}]$ denotes the probability that a variable ϵ with arbitrary m_1, m_2, f ($m_1 \neq m_2$) is less than ϵ_{th}. We initially examine calibration performance assuming no frequency offset, i.e. $f_{MT} = f_{BS} = f'_{BS}$ in (1) and (2). Afterwards, the effect of frequency offset is examined.

The previous papers have not dealt with frequency selection and refinement of calibration parameter. For comparison purpose, we consider the conventional calibration which performs relative calibration at the fixed frequencies $f^{(l)}_m$ given by

$$f^{(l)}_m = F_0 + (l-1)MB + (m-1)B \quad l = 1, \ldots, L. \tag{17}$$

The conventional calibration computes $\hat{c}_{MT,m}(f^{(l)}_m, t)$ at frequencies with constant frequency interval MB and interpolates the calibration parameters based on (13) and (14). The refinement of calibration parameter is not applied to the conventional calibration.

5.2 Effect of Frequency Selection in Calibration

Figure 4 shows the average phase error versus SNR in the conventional and proposed calibrations under $\tau = 0.1, 0.5, 1.0\,\mu$s and $T = 1$. In the figure, the proposed calibration always achieves better performance than the conventional calibration since the proposed calibration selects frequencies of good channels for channel measurements. Thus, the frequency selection is effective in improving calibration accuracy. It should be noted that the proposed and conventional calibrations have the same amount of feedback signalling because the frequency allocation does not require any additional signalling. The performance is compared under fair amount of feedback signalling.

In Fig. 4, calibration performance deteriorates as τ increases, because large τ enhances frequency selectivity in a subband leading to channel measurement degradation. In all delay spreads $\tau = 0.1$, 0.5, $1.0\,\mu$s, calibration accuracy depends on frequency allocation strategy or function J in (12). In Fig. 4, allocation 1 always outperforms allocations 2 and 3, because J in allocation 1 gives a great negative value to small $a^{(DL)}_{m,1}(f^{(l)}_m)$, which prevents the terminal from selecting a subband of poor channel condition. This property is ensured by Appendix A, which reveals that allocation 1 selects a set of less variant channels than allocations 2 and 3. Thus, allocation 1 prevents poor channels and keeps small phase error compared to allocations 2 and 3.

Figure 5 shows the 99 percentile phase error versus SNR under $\tau = 0.1, 0.5, 1.0\,\mu$s and $T = 1$. The 99 percentile phase error represents the phase error which is guaranteed with 99%. In Fig. 5, the proposed calibration always keeps better performance than the conventional calibration in terms of 99 percentile phase error. Since relative performance between the conventional and proposed calibrations in Fig. 5 is similar to that in Fig. 4, we hereafter discuss calibration performance based on the average phase error.

Figure 6 shows the average phase error versus SNR in the conventional and proposed calibrations with frequency allocation 1 under $\tau = 0.5\,\mu$s and $T = 1, 10$. In case of $T = 10$, two extreme fading scenarios are considered, i.e., fading

[†]Empirically, total group delay of RF path and analogue devices can be 10 ns order where 10 ns delay causes phase rotation of 3.6°/MHz in frequency domain.

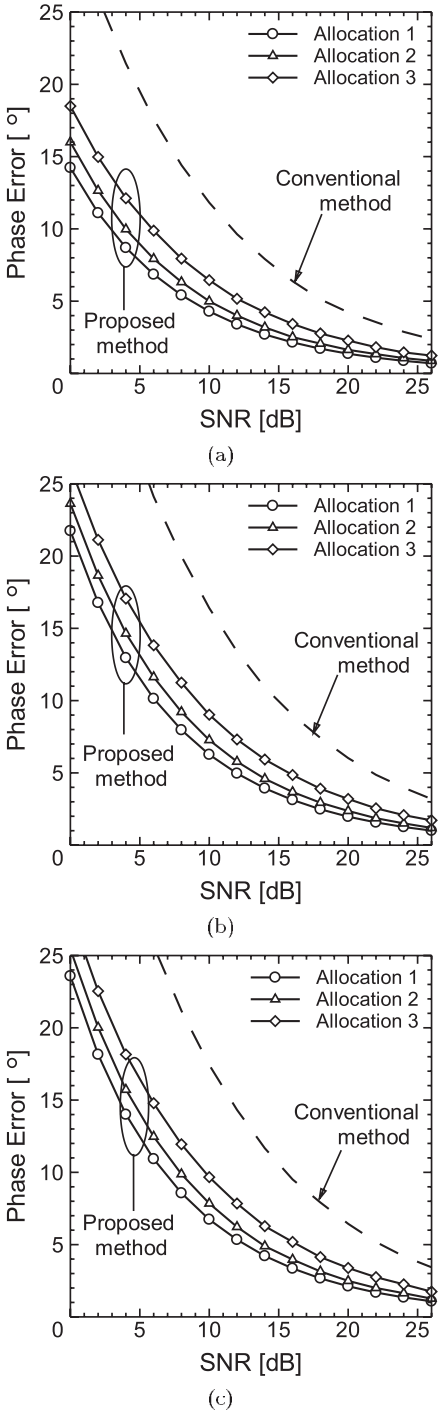

Fig. 4 Average phase error versus SNR in the conventional and proposed calibrations with $T = 1$ (a) $\tau = 0.1\,\mu$s (b) $\tau = 0.5\,\mu$s (c) $\tau = 1.0\,\mu$s.

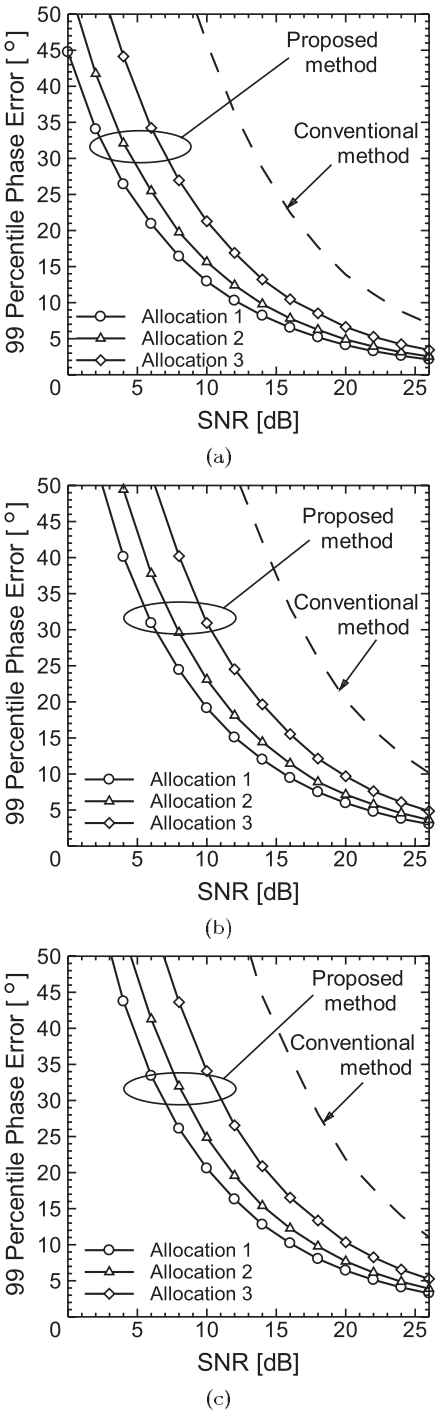

Fig. 5 99 percentile phase error versus SNR in the conventional and proposed calibrations with $T = 1$ (a) $\tau = 0.1\,\mu$s (b) $\tau = 0.5\,\mu$s (c) $\tau = 1.0\,\mu$s.

channels with perfect and zero time correlations at different time instants $t = 1, \ldots, T$. Since actual fading channel is considered as an intermediate state of the two scenarios, we can discuss actual calibration performance from the results in the two scenarios. In Fig. 6, time correlation of fading channels has little impact on performance. It implies that the calibration parameters can be refined regardless of pilot transmission cycles and the terminal's mobility. In Fig. 6, it is also seen that the proposed calibration with $T = 10$ keeps the phase error less than 10° in most cases.

Next, we examine the performance assuming no fading channels or a single direct path only. Figure 7 shows the average phase error versus SNR under no fading channels with $T = 1$. In this figure, the conventional and proposed calibrations have almost the same performance, since frequency selection does not improve channel measurement accuracy.

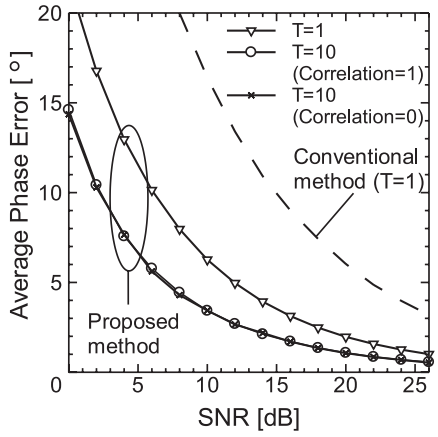

Fig. 6 Average phase error versus SNR in the conventional calibration and and the proposed calibration (allocation 1) with $T = 1, 10$ and $\tau = 0.5\,\mu$s.

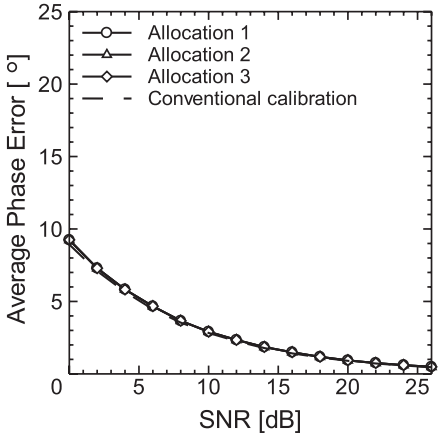

Fig. 7 Average phase error versus SNR under no fading channels with $T = 1$.

The calibration accuracy is good in both conventional and proposed calibrations. Therefore, the proposed calibration mainly helps critical situations for calibration in severe fading channels.

We have also examined many cases changing frequency offsets within $|f_{MT} - f_{BS}^{'}| \leq 20$ Hz and $|f_{BS} - f_{MT}| \leq 20$ Hz. The obtained results were the same as in Figs. 4 to 7, because the frequency offset does not influence on relative phase between the terminal's multiple antennas.

5.3 Amount of Feedback Information

In simulations, relative calibration is performed at $L = 22$ subbands for each antenna, so the total amount of feedback information with $T = 1$ corresponds to $ML(10 + 8) + 6 = 1590$ bits. Assuming update period of 1 minute for calibration, average feedback rate is 26.5 bps which is fully acceptable in high data rate wireless communications. Thus, the proposed calibration can keep low cost, low complexity, and high accuracy, using digital processing.

5.4 Impact of Calibration on Transmit Beamforming

We examine impact of calibration on transmit beamforming in MISO channel using the simulation parameters as in **5.1**.

Let us consider the terminal's transmit beamforming with $M \times 1$ weight $\boldsymbol{w}$ ($\|\boldsymbol{w}\| = 1$) after the conventional or proposed calibration. When the terminal uses the maximal ratio combining (MRC) weight, the weight $\boldsymbol{w}$ is computed as

$$\boldsymbol{w} = \tilde{\boldsymbol{a}}^{(DL)*} \tag{18}$$

with

$$\tilde{\boldsymbol{a}}^{(DL)} = \boldsymbol{a}^{(DL)} + \tilde{\boldsymbol{z}}_{MT}, \tag{19}$$

where $\boldsymbol{a}^{(DL)} = [a_{1,1}^{(DL)}, \ldots, a_{M,1}^{(DL)}]^T$, $\tilde{\boldsymbol{z}}_{MT} = [\tilde{z}_{MT,1}, \ldots, \tilde{z}_{MT,M}]^T$, $\tilde{z}_{MT,m}$ denotes the remaining noise in downlink channel estimation at the terminal's m-th antenna, and * denotes the complex conjugate. We assume $|\boldsymbol{a}^{(DL)}|^2 / E[|\tilde{\boldsymbol{z}}_{MT}|^2] = \alpha \cdot SNR$, where $\alpha (\geq 1)$ depends on noise reduction effect obtained by averaging the channel estimation parameter over downlink pilot symbols (see Appendix B).

Figure 8 shows the terminal's MRC transmit beam gain G in direction to $\boldsymbol{a}^{(UL)} = [a_{1,1}^{(UL)}, \ldots, a_{M,1}^{(UL)}]^T$ after the conventional calibration or the proposed calibration (frequency allocation 1) with $T = 1$ and $\tau = 0.5\,\mu$s. The beam gain G here is defined as

$$G = M \left| \frac{\hat{\boldsymbol{w}}^T \boldsymbol{a}^{(UL)}}{\|\hat{\boldsymbol{w}}\| \cdot \|\boldsymbol{a}^{(UL)}\|} \right|^2 .$$

In Fig. 8, ideal MRC transmit beam gain is 6 dB obtained by $M = 4$ antennas at terminal. However, actual beam gain G is less than 6 dB due to imperfect calibration and imperfect transmit weight $\boldsymbol{w}$. In case of a small α, imperfect transmit weight $\boldsymbol{w}$ which is common to the conventional and proposed calibrations is a dominant factor of degrading the beam gain due to large error $\tilde{\boldsymbol{z}}_{MT,m}$. In contrast, calibration accuracy has a large impact on the beam gain as α increases. Therefore, the proposed calibration has remarkable advantage in case of a large α such as $\alpha = 5$ or 10 dB.

Next, let us consider another case in which the terminal uses the zero-forcing (ZF) weight $\boldsymbol{w}$ of

$$\boldsymbol{w} = \left(\boldsymbol{I} - \frac{\tilde{\boldsymbol{a}}^{(DL)} \tilde{\boldsymbol{a}}^{(DL)\dagger}}{\|\tilde{\boldsymbol{a}}^{(DL)}\|^2} \right)^* \boldsymbol{b}^* \tag{20}$$

where $\boldsymbol{b}$ is the $M \times 1$ response vector of access BS and $\boldsymbol{I}$ is the identity matrix. This zero-forcing weight can be used when the terminal transmits a signal to access BS minimizing interference to near-by BS. For instance, the near-by BS could be a small base station or a femto base station. In (20), the terminal estimates channel $\tilde{\boldsymbol{a}}^{(DL)\dagger}$ and $\boldsymbol{b}$ using downlink pilot signals from the near-by BS and the access BS, respectively.

Figure 9 shows the terminal's ZF transmit beam gain G

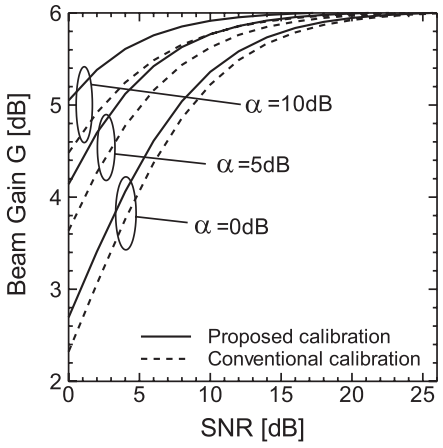

Fig. 8 Terminal's MRC transmit beam gain G in direction to $\boldsymbol{a}^{(UL)} = [a_{1,1}^{(UL)}, \ldots, a_{M,1}^{(UL)}]^T$ after the conventional calibration or the proposed calibration (allocation 1) with $T = 1$ and $\tau = 0.5\,\mu$s.

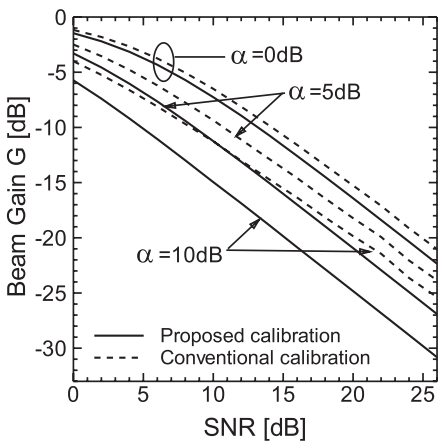

Fig. 9 Terminal's ZF transmit beam gain G in direction to $\boldsymbol{a}^{(UL)}$ after the conventional calibration or the proposed calibration (allocation 1) with $T = 1$ and $\tau = 0.5\,\mu$s.

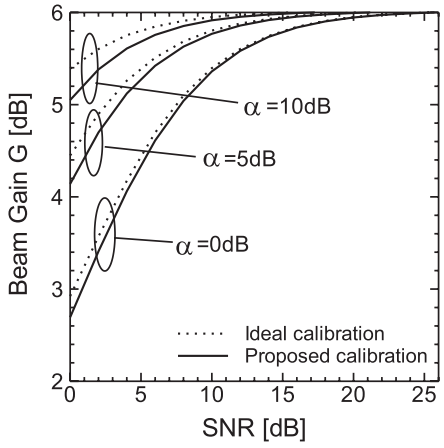

Fig. 10 Terminal's MRC transmit beam gain G in direction to $\boldsymbol{a}^{(UL)} = [a_{1,1}^{(UL)}, \ldots, a_{M,1}^{(UL)}]^T$ after ideal calibration or the proposed calibration (allocation 1) with $T = 1$ and $\tau = 0.5\,\mu$s.

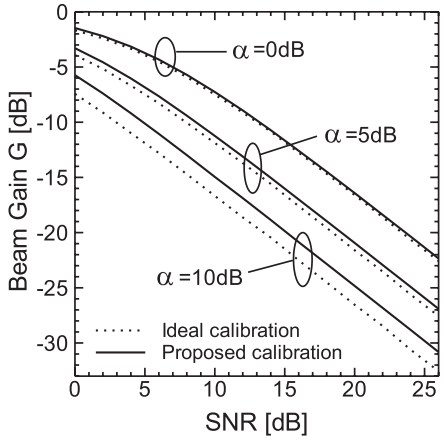

Fig. 11 Terminal's ZF transmit beam gain G in direction to $\boldsymbol{a}^{(UL)}$ after ideal calibration or the proposed calibration (allocation 1) with $T = 1$ and $\tau = 0.5\,\mu$s.

in direction to the near-by BS with the same parameters as in Fig. 8, where all elements in $\boldsymbol{b}$ are assumed as independent complex Gaussian variables. In Fig. 9, ideal ZF transmit beam gain is $-\infty$ dB, i.e., perfect nullification. However, actual beam gain is between -35 dB and 0 dB in Fig. 9 due to imperfect calibration and transmit weight. The performance gap of the proposed and conventional calibrations becomes large as α increases, because calibration accuracy has a large impact on beam accuracy. In Fig. 9, the performance gap of the two calibrations in dB is larger than in Fig. 8, because nullification is more sensitive to phase errors. Although achievable beam gain greatly depends on application scenarios, the proposed calibration always outperforms the conventional calibration.

Finally, we compare transmit beam gain between the proposed and ideal calibrations. Figure 10 shows the terminal's MRC transmit beam gain G in direction to $\boldsymbol{a}^{(UL)} = [a_{1,1}^{(UL)}, \ldots, a_{M,1}^{(UL)}]^T$ using the same parameters as in Fig. 8. In this figure, the proposed calibration keeps loss of beam gain within 0.4 dB compared to ideal calibration. Figure 11 shows the terminal's ZF transmit beam gain in direction to the near-by BS using the same parameters as in Fig. 9. The proposed calibration keeps loss of beam gain within 2 dB compared to ideal calibration.

While the proposed calibration has large phase error more than 20° at SNR = 0 dB in Fig. 4, its impact on transmit beam gain is limited in Figs. 10 and 11. This is because phase error in channel estimation for transmit weight $\boldsymbol{w}$ is larger than calibration phase error. If SNR for calibration is equal to or higher than SNR of channel estimation for transmit weight $\boldsymbol{w}$, the proposed calibration maintains small performance degradation even at low SNR. Thus, using an appropriate operation, the proposed calibration is expected to be capable of supporting terminals even at cell edges.

6. Conclusion

We have proposed an efficient antenna array calibration technique using frequency selection in OFDMA/TDD sys-

tems. In the proposed calibration, frequencies are selected for accurate channel measurements and the relative calibration is performed at the selected frequencies. Numerical results show that the proposed calibration always outperforms the conventional calibration in fading channels. Furthermore, a good strategy for frequency selection was clarified among three possible strategies. The proposed calibration is feasible in terms of accuracy, cost, and amount of control signalling. Therefore, the proposed method is a promising technology to exploit channel reciprocity in OFDMA/TDD systems.

References

[1] Y. Hara, A. Taira, and K. Oshima, "OFDMA/TDD/MIMO system with spatial scheduling," Proc. VTC2007 Spring, April 2007.
[2] K. Nishimori, K. Cho, Y. Takatori, and T. Hori, "A novel con figuration for realizing automatic calibration of adaptive array using dispersed SPDT switches for TDD systems," IEICE Trans. Commun., vol.E84-B, no.9, pp.2516–2522, Sept. 2001.
[3] A. Bordoux, B. Come, and N. Khaled, "Non-reciprocal transceivers in OFDM/SDMA systems: Impact and mitigation," Proc. IEEE RAWCON'03, Aug. 2003.
[4] D.H. Lee and C.S. Pyo, "RF performance and effect of calibration in smart antenna system," Proc. VTC2004 Spring, vol.1, pp.30–33, May 2004.
[5] M. S.-Perez, M. Calvo, M.L. de Haro, M. S.-Castaner, R. Martinez, L. Garcia, A. Martinez, F.J. G.-Madrid, J.L. Masa, and J.M. Serna, "Integration, measurements and calibration of a UMTS smart antenna," Proc. PIMRC 2004, vol.2, pp.1263–1267, Sept. 2004.
[6] IEEE P802.11n/D2.00, "Draft standard for information technology telecommunications and information exchange between systems — Local and metropolitan area networks — Specific requirements — Part 11: Wireless LAN medium access control (MAC) and physical layer (PHY) specifications," Feb. 2007.
[7] 3GPP R1-073908, Qualcomm Europe, "Calibration procedure for TDD beamforming," Oct. 2007.
[8] M. Guillaud, D. Slock, and R. Knopp, "A practical method for wireless channel reciprocity exploitation through relative calibration," Proc. ISSPA 2005, Sept. 2005.
[9] Y. Nouda, Y. Hara, Y. Yano, and H. Kubo, "An antenna array autocalibration method with bidirectional channel measurement for TDD systems," IEICE Technical Report, RCS2008-12, May 2008.
[10] G. Jiann-Ching and L.D. Larsson, "Modeling and evaluation of MIMO systems exploiting channel reciprocity in TDD mode," Proc. VTC'04 Fall, vol.6, pp.4265–4269, Sept. 2004.
[11] W.J. Welch, "Reciprocity theorems for electromagnetic fields whose time dependence is arbitrary," IRE Trans. Antennas Propag., vol.8, pp.68–73, Jan. 1960.
[12] H. Yuan, Y. Amano, S. Shi, M. Nakano, K. Kawamoto, T. Kenmoku, S. Isawa, T. Inoue, Y. Takeuchi, and Y. Yokai, "The temperature characteristics of feeder wires," Proc. WPMC'03, Oct. 2003.
[13] E.K.L. Hung, "Matrix-construction calibration method for antenna arrays," IEEE Trans. Aerosp. Electron. Syst., vol.36, no.3, pp.819–828, July 2000.
[14] 3GPP TS 36.211 V8.5.0, "E-UTRA; Physical channels and modulation (Release 8)," Dec. 2008.
[15] D. Mottier and L. Brunel, "Idle period shortening for TDD communications in large cells," Proc. VTC2006 Spring, May 2006.
[16] O. Edfors, M. Sandell, J.-J. van de Beek, S.K. Wilson, and P.O. Brjesson, "OFDM channel estimation by singular value decomposition, " IEEE Trans. Commun., vol.46, no.7, pp.931–939, July 1998.
[17] Y. Hara, A. Taira, L. Brunel, and T. Sälzer,"Frequency-averaged MMSE channel estimator for multicarrier transmission schemes," Proc. VTC2004 Fall, Sept. 2004.

Appendix A: Property of Function *J*

In (12), three functions J are given by

$$J = \begin{cases} \sum_{m=1}^{M} \log_{10} |\hat{a}_{m,1}^{(DL)}(f_m^{(l)})| & \text{in allocation 1} \\ \sum_{m=1}^{M} |\hat{a}_{m,1}^{(DL)}(f_m^{(l)})| & \text{in allocation 2} \\ \sum_{m=1}^{M} |\hat{a}_{m,1}^{(DL)}(f_m^{(l)})|^2 & \text{in allocation 3.} \end{cases}$$

Although all methods (allocation 1, 2, 3) attempt to select large $|\hat{a}_{m,1}^{(DL)}(f_m^{(l)})|$, they have different sensitivities to channel variation.

To get insight of behavior, let us consider a set A of two frequencies which have channel parameters $|x_1|$ and $|x_2|$ ($|x_1| \le |x_2|$) and another set B of two frequencies which have channel parameters $|X_1| = |x_1| - \rho$ and $|X_2| = |x_2| + \rho$ with $0 < \rho < |x_1|$. Since

$$\begin{aligned} \log_{10}|X_1| + \log_{10}|X_2| &< \log_{10}|x_1| + \log_{10}|x_2| \\ |X_1| + |X_2| &= |x_1| + |x_2| \\ |X_1|^2 + |X_2|^2 &> |x_1|^2 + |x_2|^2 \end{aligned} \quad (\text{A}\cdot 1)$$

allocation 1 selects set A from the two sets whereas allocation 3 selects set B. Allocation 2 selects set A or set B with equal probability. Therefore, allocation 1 selects a set of less variant channels than allocations 2 and 3.

Appendix B: Signal Transmission Model

Consider the BS transmits the p-th symbol $s(p)$ ($E[|s(p)|^2] = 1$) with $c_{BS,1} = 1$. Then, the recei ved symbol at the terminal is expressed as

$$y_{m,1}(p) = a_{m,1}^{(DL)} s(p) + z_{MT,m}(p) \quad (\text{A}\cdot 2)$$

where $a_{m,1}^{(DL)}$ is the complex channel parameter defined in (3) and $z_{MT,m}(p)$ is the white noise with power $P_{MT,z}$ ($= E[|z_{MT,m}(p)|^2]$). The BS's transmit power $P_{BS,s}$ is given by $|a_{m,1}^{(DL)}|^2$. When the terminal estimates $a_{m,1}^{(DL)}$ using p_0 time pilot symbols, the estimated parameter $\tilde{a}_{m,1}^{(DL)}$ is represented by

$$\tilde{a}_{m,1}^{(DL)} = \frac{1}{p_0}\sum_{p=1}^{p_0} y_{m,1}(p)s(p)^* = a_{m,1}^{(DL)} + \tilde{z}_{MT,m}$$

$$\tilde{z}_{MT,m} = \frac{1}{p_0}\sum_{p=1}^{p_0} z_{MT,m}(p)s(p)^*$$

where $\tilde{z}_{MT,m}$ is the remaining noise in channel estimation. Then, we have

$$\frac{|a_{m,1}^{(DL)}|^2}{E[|\tilde{z}_{MT,m}|^2]} = p_0 \cdot \frac{P_{BS,s}}{P_{MT,z}} = p_0 \cdot \text{SNR}. \quad (\text{A}\cdot 3)$$

In OFDMA, the channel estimation parameter can be also weighted and averaged over frequency domain [16], [17]. Therefore, we use the following general expression for performance evaluation:

$$\frac{|a_{m,1}^{(DL)}|^2}{E[|\tilde{z}_{MT,m}|^2]} = \alpha \cdot \mathrm{SNR}. \qquad (\mathrm{A}\cdot 4)$$

Yoshitaka Hara received the B.E., M.E., and Dr.Eng. degrees from the University of Tokyo, Tokyo, Japan, in 1993, 1995, and 2003, respectively. In 1996, he joined Mitsubishi Electric Corporation. From April 1999 to December 2001, he was also with YRP Mobile Telecommunications Key Technology Research Laboratories Co., Ltd. From September 2003 to October 2006, he was with Mitsubishi Electric Information Technology Centre Europe B.V. (ITE) in France. Since October 2006, he has been a head researcher at Mitsubishi Electric Corporation, Information Technology R&D Center in Japan. His research interests include wireless transmission schemes and multiantenna techniques. He is a recipient of the Telecom System Technology Award from the Telecommunication Advancement Foundation in 2001 and the IEICE Transactions Best Paper Awards in 2002 and 2006.

Yasuhiro Yano was born in Saitama, Japan. He received the B.S. and M.S. degrees in electrical engineering from Saitama University, Saitama, Japan, in 1990 and 1992, respectively. He has been with Mitsubishi Electric Corporation, Kanagawa, Japan, since 1992, where he has been engaged in research and development on telecommunication systems. He is currently a manager of Wireless Signal Processing Team in the Information Technology R&D Center.

Hiroshi Kubo received the B.E., M.E. and Dr.Eng. degrees in communication engineering from Osaka University, Osaka, Japan in 1984, 1986 and 1996, respectively. He has been with Mitsubishi Electric Corporation, Kanagawa, Japan, since 1986, where he has been engaged in research and development on digital mobile radio, optical and digital subscriber loop communication systems. He is currently a senior manager of the Wireless Communication Technology Department in the Information and Technology R&D Center. His research interests include digital communications and digital signal processing. He is a member of the IEICE of Japan and the Society of Information Theory and Its Application of Japan.